Int. J. Electrochem. Sci., 10 **(2015)** 46 - 62

International Journal of
ELECTROCHEMICAL
SCIENCE
www.electrochemsci.org

Gundelia tournefortii as a Green Corrosion Inhibitor for Mild Steel in HCl and H_2SO_4 Solutions

N. Soltani[1,*], *M. Khayatkashani*[2]

[1]Department of Chemistry, Payame Noor University, P.O. Box 19395-3697 Tehran, Iran
[2]Department of Analytical Chemistry, Faculty of Chemistry, University of Kashan, Kashan, I.R., Iran
[*]E-mail: nasrin.soltani@pnu.ac.ir; nasrin_soltani2056@yahoo.com

Received: 16 July 2014 / *Accepted:* 17 October 2014 / *Published:* 17 November 2014

The inhibitive action of leaf extract of *Gundelia tournefortii* (*G. tournefortii*) on mild steel corrosion in 2.0 M HCl and 1.0 M H_2SO_4 solutions was studied using weight loss measurement, potentiodynamic polarization and electrochemical impedance spectroscopy (EIS) techniques. The inhibition efficiency was found to increase with increase of the inhibitor concentrations due to the adsorption of the inhibitor molecules on the metal surface. In addition, it was established the Langmuir adsorption isotherm fits well with the experimental data. The inhibition efficiency was found to be 93% and 90% at 150 ppm in 2.0 M HCl and 1.0 M H_2SO_4 respectively. Cathodic and anodic polarization curves show that *G. tournefortii* extract is a mixed-type inhibitor in both acidic media.EIS showed that the charge transfer controls the corrosion process. The effect of temperature on the inhibition efficiency was studied.Finally, inhibition efficiency of *G. tournefortii* extract was discussed in terms of adsorption and protective film formation.

Keywords: Electrochemistry; Corrosion inhibition; *Gundelia tournefortii* extract; Mild steel; HCl; H_2SO_4

1. INTRODUCTION

Acid solutions are widely used in industry, some of the important fields of application being acid pickling of iron and steel, chemical cleaning and processing, ore production and oil well acidification [1]. The use of inhibitor is one of the most practical methods for protecting metals against corrosion and it, in these days, becomes increasingly popular. Most well-known acid inhibitors are organic compounds containing nitrogen, sulfur, and oxygen atoms [2-5]. Nevertheless, the use of chemical inhibitors has been limited because of the environmental threat. In the 21st century, the research in the field of ‘‘green’’ or ‘‘eco-friendly’’ corrosion inhibitors has been addressed toward the goal of using cheap, effective compounds at low or ‘‘zero’’ environmental impact [6]. Some investigations have in recent time been made into the corrosion inhibiting properties of natural

products of plant origin, which have been found to generally exhibit good inhibition efficiencies [7-11]. Extracts of naturally occurring products contain mixtures of compounds and are biodegradable in nature. These compounds having nitrogen and sulfur as constituent atoms were studied as corrosion inhibitor in HCl medium [12]. Recently, natural products, for example, lupine extract [13], *Gossipiumhirsutum L*. extract [7], *Murrayakoenigii* leaves extract [10], *Punicagranatum* extract [14], *Dacryodisedulis* extract [15], damsissa (*Ambrosia maritime*, L.) extract [16], *Oxandraasbeckii* extract [17], *Phyllanthusamarus* extract [18], seed extract of *Psidiumguajava* [19], *Launaea nudicaulis* extract [20], and *Artemisia pallens* (Asteraceae) extract [21] all have been reported to be effective in reducing the corrosion rate of metals in acidic media. Oguzie et al. [22] studied the inhibitive action of plants materials include leaf extracts *Occimumviridis*, *Telferiaoccidentalis*, *Azadirachtaindica* and *Hibiscus sabdariffa* as well as extracts from the seeds of *Garcinia kola* on mild steel corrosion in HCl and H_2SO_4 solutions.

Gundeliatournefortii L. from the Compositae family is a plant native to Asian-temperate zones of Western Asia, namely Cyprus, Egypt, Iran and Turkey. *G. tournefortii* is an important food source and a well-known medicinal plant locally known as "Kangar" in Iran. *G. tournefortii* is found as a wild herb growing during late winter and early spring on the hills in western and southern parts of Iran. Total phenolic contents and the antioxidant activities of *G. tournefortii* have been investigated. However, not much attention has been paid to this extract as a source of corrosion inhibitor.

The aim of this study is to investigate the ability of *G. tournefortii*as friendly and environmentally safe inhibitors to protect the mild steel against corrosion in 2.0 M HCl and 1.0 M H_2SO_4 solutions. The investigation of corrosion parameters was performed by weight loss, electrochemical polarization measurements and electrochemical impedance spectroscopy. Effects of inhibitor concentration, temperature and immersion time on inhibition action were fully investigated. The adsorption isotherm of inhibitor on steel surface and apparent activation energy (E_a) are obtained.

2. EXPERIMENTAL

2.1. Extract preparation

G. tourneofortti L. extract were purchased from the traditional medicine department of the Barij Essence Pharmaceutical Company (Kashan, Iran). The extract was prepared according to the following procedure [23]; the aerial parts of *G. tourneofortti* L. were gathered in around of Kashan, Iran, in June 2011. A 0.5 g amount of powdered sample was extracted with 40 mL methanol- water mixture (7:3 v/v) under reflux (80 ºC) for 1 h. The solution was filtered into a 50 mL volumetric flask and residue washed with 10 mL the solvent and added to previous solution.

2.2. Corrosion studies

2.2.1. Test solutions

1.0 M HCl and 0.5 M H_2SO_4 solutions were prepared by dilution of 37% HCl (Merck) and 98% H_2SO_4 (Merck) using distilled water. The concentration range of *G. tourneofortti* L. extract employed

was varied from 25 to 150 ppm. This concentration range was chosen upon the maximum solubility of *G. tourneofortti* L. extract. The powder extract was first dissolved in 1% (v/v) methanol before it was diluted with 1.0 M HCl and 0.5 M H_2SO_4 solutions.

2.2.2. Preparation of working electrodes

The corrosion tests were carried out on an electrode or specimens of mild steel with the following composition (by weight, wt.%): C (0.027), Si (0.0027), P (0.009), Al (0.068), Mn (0.340), S (0.007), Nb (0.003), Cu (0.007), Ni (0.030), Ti (0.003), Cr (0.008), V (0.003) and the remainder iron. Coupons were cut into 1 cm× 1 cm × 0.2 cm dimensions used for weight loss measurements. For polarization and electrochemical impedance studies, the metal was soldered with Cu-wire for electrical connection and was embedded in epoxy resin to expose a geometrical surface area of 1 cm^2 to the electrolyte. The electrodes were abraded with a series of silicon carbide abrasive paper (grade 400, 800,1000, 1200) degreased with acetone, and rinsed in distilled water before they were inserted into the test solution.

2.2.3. Weight loss experiment

Weight loss experiments were performed (in triplicate) in a double walled glass cell equipped with a thermostat-cooling condenser. The temperature was adjusted to 25 ± 0.1°C using MEMERT thermostat. The weight loss of steel in 2.0 M HCl and 1.0 M H_2SO_4 (in mg cm^{-2} h^{-1}) with and without the addition of inhibitors were determined at different immersion times at 25°C by weighing the cleaned samples before and after hanging the coupon into 50 cm^3 of the solution. The experiments were repeated at different temperatures, ranging from 35–65 °C in the absence and presence of 1.00 mM inhibitors after 1 h of immersion time. The corrosion rate (υ) and the inhibition efficiency η_w (%) were calculated from equations (1) and (2):

$$v = \frac{(m_1 - m_2)}{(S \times t)} \quad (1)$$

$$\eta_w(\%) = \frac{(v_0 - v)}{v_0} \times 100 \quad (2)$$

Where m_1 is the mass of the specimen before corrosion, m_2 the mass of the specimen after corrosion, *S*, the total area of the specimen, *t*, corrosion time, υ_0 and υ are the corrosion rates of the specimen in acid solutions without and with the addition of inhibitor, respectively.

2.2.4. Electrochemical measurements

Polarization and impedance measurements were performed using AUTOLAB PGSTAT 35 model potentiostat–galvanostat. The polarization and impedance data were analyzed using GPES software and FRA software, respectively. A three electrode cell assembly consisting of mild steel working electrode (WE), platinum rod as counter electrode (CE) and a silver–silver chloride

(Ag/AgCl) electrode as reference electrode (RE) containing 300 mL of electrolyte were used for electrochemical measurement. The temperature of the electrolyte was maintained at room temperature (25 °C). The electrodes were immersed for 30 min to obtain steady state open circuit potential. Tafel polarization curves were recorded at constant sweep rate of 0.5 mV/s and the scanning range was from -500 to +500 mV with respect to the open circuit potential. Electrochemical impedance spectroscopy measurements were performed at corrosion potentials, E_{corr}, over a frequency range of 100 kHz to 0.1 Hz with a signal amplitude perturbation of 5 mV. The measurements were repeated three times for each condition and the average values were presented. The impedance diagrams are given in Nyquist representation. The polarization and impedance parameters such as corrosion current densities (I_{corr}), corrosion potential(E_{corr}), anodic Tafel slope (b_a) and cathodicTafel slope (b_c) double layer capacitance (C_{dl}), charge transfer resistance (R_{ct}), were computed from the polarization curves and Nyquist plots.

The inhibition efficiency values were calculated from potentiodynamic polarization measurements using the equation (3),

$$\eta_{pol}(\%) = (\frac{I_0 - I}{I_0}) \times 100 \quad (3)$$

where I_0 and I are the corrosion current densities in absence and presence of inhibitor, respectively.

From impedance measurements the inhibition efficiency values were calculated using charge transfer resistance as follows:

$$\eta_{EIS}(\%) = \frac{(1/R_{ct}^0) - (1/R_{ct})}{(1/R_{ct}^0)} \times 100 \quad (4)$$

where R^0_{ct} and R_{ct} are the charge transfer resistance values without and with inhibitor, respectively.

3. RESULT AND DISCUSSION

3.1. Gravimetric results

The weight loss method of monitoring corrosion rate is useful because of its simple application and reliability [24]. Therefore, a series of weight loss measurements were carried out after 2 h immersion in 2.0 M HCl and 1.0 M H_2SO_4 solutions in the absence and presence of various concentrations of *G. tournefortii* extract. Table 1 shows the calculated values of corrosion rates obtained using Eq. (1) as well as inhibition efficiency values evaluated using the expression given in Eq. (2). The results show that the corrosion efficiencies in each acid medium increase with increasing inhibitor concentration. From the Table 1, it can be seen that corrosion rate (v_{corr}) values get decreased and inhibition efficiency (η_w) increased with concentration of inhibitor. This is due to the fact that the adsorption coverage of inhibitor on mild steel surface increases with inhibitor concentration [25].

To assess the retarding behaviour of corrosion inhibitors on a time scale, weight loss measurements were carried out in 2.0 M HCl and 1.0 M H_2SO_4 solutions in absence and in presence

different concentrations of of *G. tournefortii* extract for various immersion times (2, 4, 6, 8 and 24 h) at temperature 25 ºC and the results are shown in Fig. 1.

Table 1. Corrosion parameters for mild steel in 20 M HCl and 1.0 M H_2SO4 in the presence and absence of different concentrations of *G. tournefortii* extract obtained from weight loss for 2 h at 25 ºC.

Concentration (ppm)	2.0 M HCl			1.0 M H_2SO_4		
	v (mg cm^{-2} h^{-1})	θ	η_W (%)	v (mg cm^{-2} h^{-1})	θ	η_W (%)
Blank	1.87	-	-	2.63	-	-
25	1.1	0.41	41.2	1.58	0.40	39.9
50	0.82	0.56	56.1	0.99	0.62	62.3
75	0.52	0.60	60.0	0.69	0.74	73.8
100	0.37	0.80	80.2	0.56	0.79	78.7
125	0.21	0.89	88.8	0.38	0.86	85.6
150	0.14	0.93	92.5	0.26	0.90	90.1

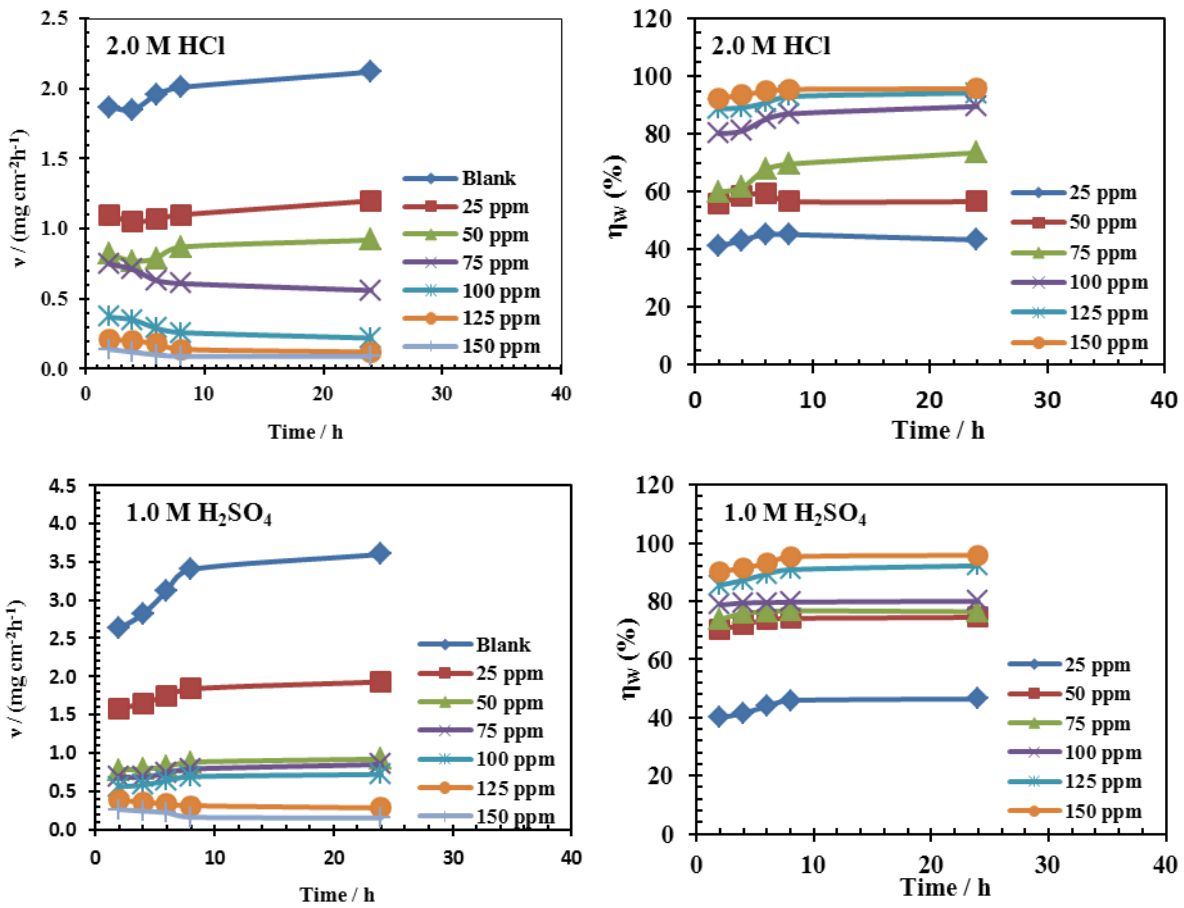

Figure 1. Relationship between corrosion rate (υ) (On the left side) and inhibition efficiency (ηw) (On the right side) with the immersion time in the absence and presence of different concentrations of G. tournefortii extract in 2.0 M HCl and 1.0 M H_2SO_4

As it is seen in Fig. 1, the inhibition efficiency of *G. tournefortii* extract in both acid solutions shows a slight increase and corrosion rate (v_{corr}) of mild steel shows a slight decrease with the increase in immersion time from 2 to 48 h. This increase in η_w % is probably due to the more or less complete surface coverage of the steel surface with inhibitor molecules and an improvement in the quality of the protective film with time [26]. This indicates *G. tournefortii* extract is a good corrosion inhibitor for mild steel in both acid media.

3.2. Potentiodynamic polarization measurements

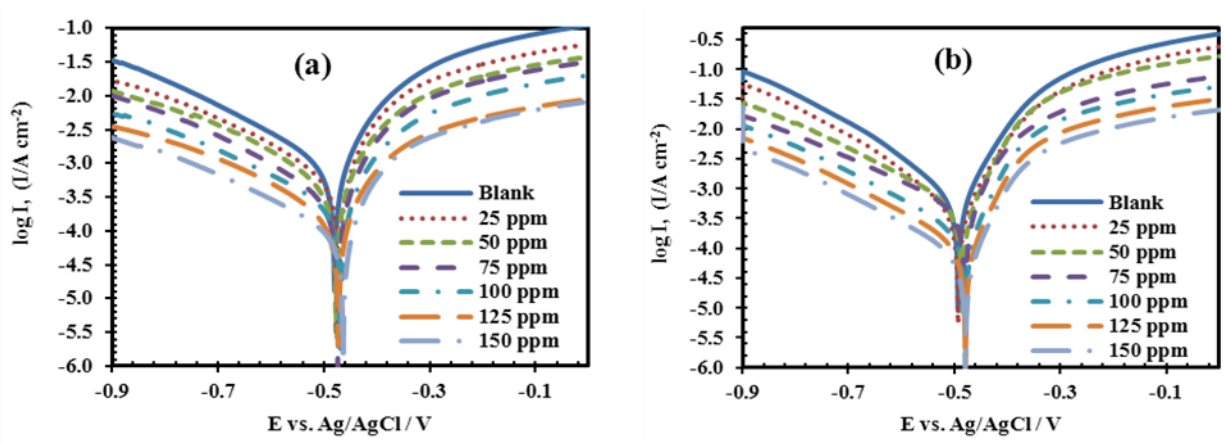

Figure 2. Polarization curves for the mild steel in (a) 2.0 M HCl and (b) 1.0 M $H_2SO_4$with different concentration of *G. tournefortii* extract

Table 2. Polarization parameters for mild steel in 2.0 M HCl and 1.0 M H_2SO_4 in the presence and absence of *G. tournefortii* extract.

Acid solution	Concentration (ppm)	$-E_{corr}$ (mV, vs. Ag/AgCl)	$-b_c$ (mV dec^{-1})	b_a (mV dec^{-1})	I_{corr} (µA cm^{-2})	η_p (%)
2.0 M HCl	Blank	480	218	85	841.4	-
	25	478	230	90	483.8	42.5
	50	477	264	88	350.8	58.3
	75	473	237	70	309.6	63.2
	100	471	206	110	154.0	81.7
	125	469	220	92	87.5	89.6
	150	463	231	103	53.0	93.7
1.0 M H_2SO_4	Blank	493	160	77	1093.8	-
	25	493	165	80	649.7	40.6
	50	485	192	84	363.7	64.0
	75	479	198	67	379.5	74.5
	100	479	183	70	231.3	78.9
	125	478	194	72	155.9	85.8
	150	478	163	64	101.7	90.7

Potentiodynamic polarization curves of mild steel in 2.0 M HCl and 1.0 M H_2SO_4 in the absence and presence of *G. tournefortii* extract are presented in Fig 2 a, b. The corrosion kinetic parameters obtained from these curves are depicted in Table 2. It is apparent from the figure that, both the anodic and cathodic branches of the polarization curves of the acid solutions shifted towards lower current density at all investigated concentrations in both acid media. This indicates that both the anodic and cathodic reactions (metal dissolving and hydrogen evolution) of mild steel corrosion were inhibited by *G. tournefortii* extract in 2.0 M HCl and 1.0 M solution. With the addition of inhibitor, the E_{corr} values shifted towards less positive direction and also there is no significant variation in b_a and b_c values. This suggests that *G. tournefortii* extract behaves as mixed type inhibitor [27]. The protection efficiency increases and corrosion current density decreases with increasing concentration of inhibitor in both acid media. But the inhibition performance of *G. tournefortii* extract is better in 2.0 M HCl compared to 1.0 M H_2SO_4.

3.3. Electrochemical impedance spectroscopy measurements

The corrosion behaviour of mild steel in 2.0 M HCl and 1.0 M H_2SO_4 in the absence and presence of *G. tournefortii* extract were evaluated by electrochemical impedance spectroscopy. The impedance data are presented in the form of Nyquist plots in Fig. 3 a, b.

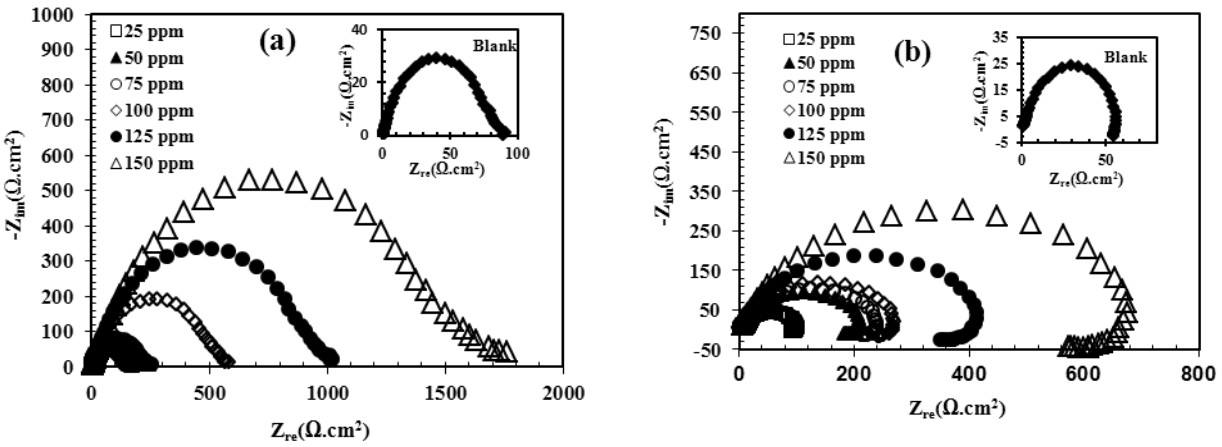

Figure 3. Nyquist plots for mild steel in (a) 2.0 M HCl and (b) 1.0 M H_2SO_4 with different concentration of *G. tournefortii* extract

As shown in Fig. 3 a, in uninhibited and inhibited 2.0 M HCl solutions, the impedance spectra exhibit one single capacitive loop, which indicates that the corrosion of steel is mainly controlled by the charge transfer process [6]. On the other hand, in 1.0 M H_2SO_4 solution, the impedance spectra shown in Fig. 3 b consist of two loops, one large capacitive loop at high frequencies (HF), and one small inductive loop at low frequencies (LF). The capacitive loop at HF is generally related to the charge transfer of the corrosion process and double layer behavior. In contrast, the inductive loop at LF may be attributed to the relaxation process obtained by adsorption species like $FeSO_4$ [28] or inhibitor

species [29] on the electrode surface. In both acids, with respect to blank solution, the shape is maintained throughout all tested concentrations, indicating that there is almost no change in the corrosion mechanism occurs regardless of the inhibitor addition [30].

EIS spectra in both acids are simulated using the equivalent circuit in Fig. 4, which represents a single charge transfer reaction. Generally this circuit falls into the classic parallel capacitor and resistor combination. The simplest fitting is represented by Randles equivalent circuit (Fig. 4), which is a parallel combination of the charge-transfer resistance (R_{ct}) and the constant phase element (CPE), both in series with the solution resistance (R_s). The semicircles are observed to be depressed into the Z_{real} of the Nyquist plot as a result of the roughness of the metal surface [14, 15]. It is modelled by a power-law-dependent capacity term known as the constant phase element (CPE). This kind of phenomenon is known as the "dispersing effect" [31, 32].

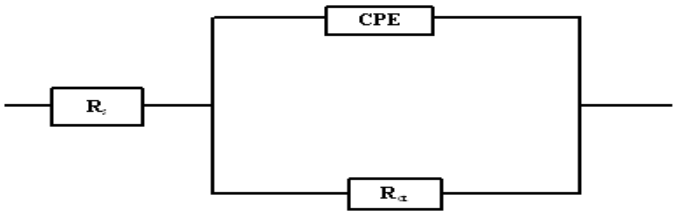

Figure 4. Electrical equivalent circuit model used to fit impedance data.

Considering that the impedance of a double layer does not behave as an ideal capacitor in the presence of a dispersing effect, a CPE is used as a substitute for the capacitor in Fig. 4 to fit more accurately the impedance behaviour of the electric double-layer. Constant phase elements have widely been used to account for deviations brought about by surface roughness. The impedance of CPE is given by Eq. (5):

$$Z_{CPE} = \frac{1}{Y_0} \times \frac{1}{(j\omega)^n} \quad (5)$$

where Y_0 is the magnitude of the CPE, n the CPE exponent (phase shift), ω the angular frequency ($\omega = 2\pi f$, where f is the AC frequency), and j here is the imaginary unit. Depending on the value of the exponent n, Q may be a resistance, R $(n = 0)$; a capacitance, $C(n = 1)$; a Warburg impedance, $W(n = 0.5)$ or an inductance, $L(n = -1)$ [30]. When the value of n is 1, the CPE behaves like an ideal double-layer capacitance (C_{dl}). The correction of capacity to its real values is calculated from the Eq. (6):

$$C_{dl} = Y_0(\omega_{max})^{n-1} \quad (6)$$

where ω_{max} is the frequency at which the imaginary part of impedance ($-Z_{im}$) has a maximum [32]. The data obtained from fitted spectra are listed in Table 3. Data in Table 3 show that the R_s values are very small in comparison with the R_{ct} values. By increasing the inhibitor concentrations, the R_{ct} values increase and the calculated C_{dl} values decrease. This decrease in C_{dl} results from a decrease in local dielectric constant and/or an increase in the thickness of the double layer, suggesting that Schiff bases inhibit the iron corrosion by adsorption at steel/acid interface [31]. It is well known that the capacitance is inversely proportional to the thickness of the double layer [32]. A low capacitance

may result if water molecules at the electrode interface are largely replaced by organic inhibitor molecules through adsorption [33]. The larger inhibitor molecules also reduce the capacitance through the increase in the double layer thickness. The thickness of this protective layer increases with increase in inhibitor concentration. This process results in a noticeable decrease in C_{dl}. This trend is in accordance with Helmholtz model, given by the following equation:

$$C_{dl} = \frac{\varepsilon\varepsilon_0 A}{d} \quad (7)$$

where d is the thickness of the protective layer, ε is the dielectric constant of the medium, ε_0 is the vacuum permittivity and A is the effective surface area of the electrode. As a result of the effective adsorption of the inhibitor, the value of C_{dl} is always smaller in the presence of the inhibitor than in its absence. It is apparent that causal relationship exists between adsorption and inhibition.

Table 3. Impedance data of mild steel in 2.0 M HCl and 1.0 M H_2SO_4 with and without *G. tournefortii* extract.

Acid solution	Concentration (ppm)	R_s ($\Omega.cm^2$)	R_{ct} ($\Omega.cm^2$)	Q ($\mu\Omega^{-1}$ s^n cm^{-2})	n	C_{dl} (μF cm^{-2})	η_{EIS} (%)
2.0 M HCl	Blank	0.47	85.6	553.3	0.76	5934.2	-
	25	1.3	159.7	263.7	0.77	431.6	46.4
	50	1.4	208.4	164.6	0.79	236.7	58.9
	75	1.6	240.3	150.4	0.81	220.4	64.4
	100	2.8	560.0	108.8	0.83	176.9	84.7
	125	3.5	981.2	57.8	0.84	128.7	91.3
	150	4.3	1638.2	36.9	0.87	98.7	94.8
1.0 M H_2SO_4	Blank	1.1	57.1	646.1	0.74	746.7	-
	25	1.8	97.3	442.0	0.76	563.8	41.3
	50	2.8	186.7	263.3	0.77	324.5	69.4
	75	3.9	229.6	243.9	0.78	311.8	75.1
	100	2.5	272.1	166.2	0.78	276.4	79.0
	125	2.7	405.2	138.5	0.79	223.7	85.9
	150	3.2	657.4	89.3	0.80	116.6	91.3

3.4. Effect of temperature

In general, the effect of temperature on the inhibited acid–metal reaction is highly complex, because many changes occur on the metal surface such as rapid etching and desorption of inhibitors and the inhibitor itself may undergo decomposition or rearrangement [34]. In order to calculate the activation energy of the corrosion process and investigate the mechanism of inhibition, gravimetric measurements were carried out at various temperatures (35-65 $^{\circ}$C) in the absence and presence of *G. tournefortii* extract in 2.0 M HCl and 1.0 M H_2SO_4. The results are shown in Table 4. It was found that corrosion rates of mild steel, in free and inhibited acid solutions increases with a rise in temperature.

Table 4. Corrosion parameters for mild steel in 2.0 M HCl and 1.0 M H_2SO_4 in the presence and absence of different concentrations of *G. tournefortii* extract obtained from weight loss for 2 h.

Temperature (ºC)	C (ppm)	20 M HCl			1.0 M H_2SO_4		
		ν (mg cm^{-2} h^{-1})	θ	η_w (%)	ν (mg cm^{-2} h^{-1})	θ	η_w (%)
35	Blank	2.82	-	-	3.21		
	25	1.67	0.41	40.8	2.05	0.36	36.1
	50	1.25	0.56	55.7	1.39	0.57	56.7
	75	0.81	0.71	71.3	0.95	0.70	70.4
	100	0.58	0.79	79.1	0.76	0.76	76.3
	125	0.37	0.86	86.2	0.58	0.82	81.9
	150	0.29	0.90	89.7	0.39	0.88	87.9
45	Blank	3.12	-	-	4.87		
	25	1.89	0.39	39.4	3.22	0.34	33.9
	50	1.45	0.54	53.5	2.24	0.54	54.0
	75	0.98	0.69	68.6	1.65	0.66	66.1
	100	0.68	0.78	78.2	1.25	0.74	74.3
	125	0.49	0.84	84.3	0.96	0.80	80.3
	150	0.35	0.89	88.8	0.67	0.86	86.2
55	Blank	4.65	-	-	8.23		
	25	2.84	0.39	38.9	5.74	0.30	30.3
	50	2.23	0.52	52.0	4.24	0.48	48.5
	75	1.48	0.68	68.2	3.25	0.61	60.5
	100	1.1	0.76	76.3	2.66	0.68	67.7
	125	0.79	0.83	83.0	2.14	0.74	74.0
	150	0.56	0.88	88.0	1.57	0.81	80.9
65	Blank	6.62	-	-	12.65		
	25	4.36	0.34	34.1	8.92	0.29	29.5
	50	3.24	0.51	51.1	6.89	0.46	45.5
	75	2.34	0.65	64.7	5.49	0.57	56.6
	100	1.82	0.73	72.5	4.47	0.65	64.7
	125	1.39	0.79	79.0	3.69	0.71	70.8
	150	0.98	0.85	85.2	2.85	0.77	77.5

The dependence of the corrosion rate on temperature can be expressed by the Arrhenius equation. The Arrhenius equation could be written by Eq. 8, 9 [32].

$$\nu_{corr}^{0} = K^{0} \exp(-\frac{E_a^0}{RT}) \quad (8)$$

$$\nu_{corr} = K \exp(-\frac{E_a}{RT}) \quad (9)$$

where v_{corr} and v^0_{corr} is corrosion rate which is obtained from Table 4, K and K^0 is the Arrhenius pre-exponential factor, R is the gas constant E_a is the apparent activation energy of the corrosion reaction, T is the absolute temperature. The activation energy could be determined from Arrhenius plots presented in Fig. 5. The results are shown in Table 5.

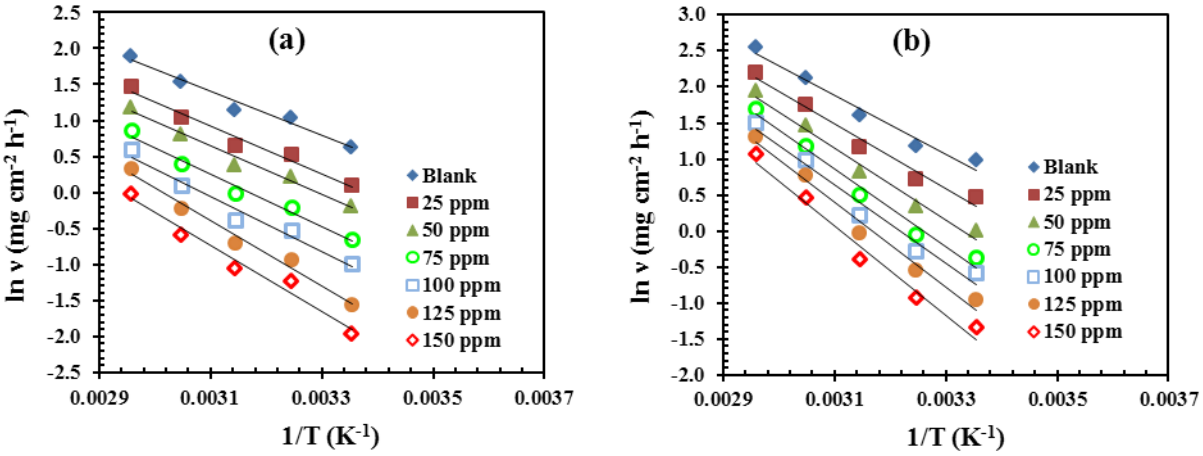

Figure 5. Arrhenius plots of ln v_{corr} versus 1/T in the absence and presence of different concentration of *G. tournefortii* extract in (a) 2.0 M HCl, (b) 1.0 M H2SO4.

It is clear that the activation energy increases in presence of *G. tournefortii* extract and consequently the rate of corrosion decreases. The lower value of the activation energy of the process in an inhibitor's presence when compared to that in its absence is attributed to its chemisorption while the opposite is the case with physical adsorption [36]. In the both acid solutions, it was found that values E_a for inhibited systems are higher than those of uninhibited systems and the results were attributed to physical adsorption [36, 37]. The higher E_a value in the inhibited solution can be correlated with the increased thickness of the double layer, which enhances the activation energy of the corrosion process [38].

An alternative formulation of Arrhenius equation is [33]:

$$v_{corr} = \frac{RT}{N_A h}\exp(\frac{\Delta S^*}{R})\exp(-\frac{\Delta H^*}{RT}) \qquad (10)$$

where v_{corr} is the corrosion rate obtained from gravimetric measurements, h is Planck's constant, N_A Avogadro's number, R the universal gas constant, ΔH^* the enthalpy of the activation and ΔS^* is the entropy of activation. Fig. 6 shows a plot of $\ln(v/T)$ against $1/T$. Straight lines are obtained with a slope of $(-\Delta H^*/R)$ and an intercept of $(\ln(R/Nh) + (\Delta S^*/R))$ from which the values of ΔH^* and ΔS^* are calculated and listed in Table 5. The positive signs of ΔH* reflect the endothermic nature of the mild steel dissolution process. The analysis of results of Table 8 shows that the values of E_a and ΔH^* enhance with the inhibitor suggesting that the energy barrier of corrosion reaction increases with presence of PG extract. This means that the corrosion reaction will further be pushed to surface sites that are characterized by progressively higher values of E_a in the presence of the inhibitor [33].

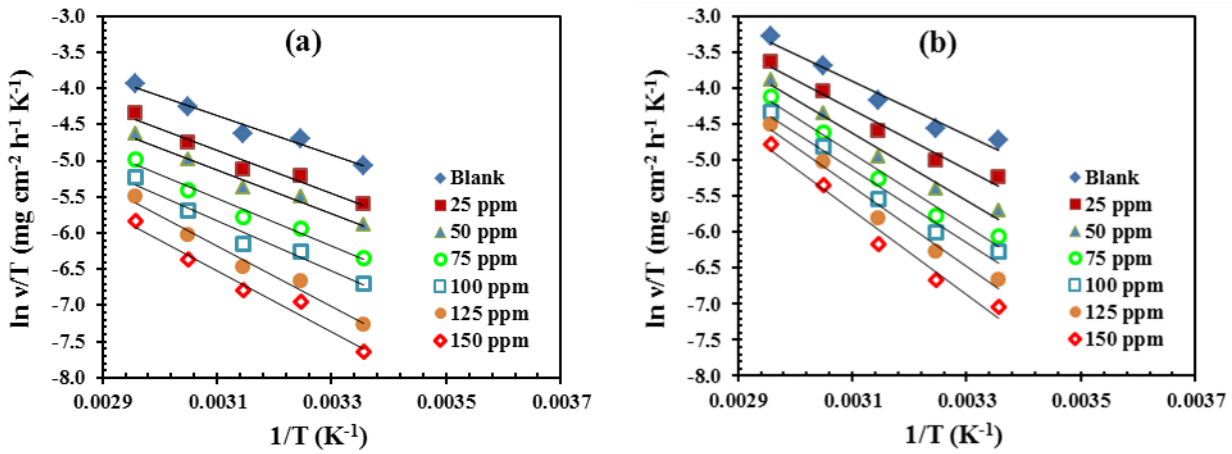

Figure 6. Arrhenius plots of ln (v_{corr}/T) versus $1/T$ in the absence and presence of different concentrations of *G. tournefortii* extract in (a) 2.0 M HCl and (b) 1.0 M H_2SO_4.

Table 5. Activation parameters, Ea, ΔH*, ΔS *, of the dissolution of mild steel in 2.0 M HCl and 1.0 M H_2SO_4 in the absence and presence of *G. tournefortii* extract.

Acid solution	Concentration (ppm)	E_a (kJ mol^{-1})	ΔH^* (kJ mol^{-1})	ΔS^* (J $mol^{-1}K^{-1}$)
2.0 M HCl	Blank	25.3	22.7	-163.7
	25	27.4	24.8	-161.1
	50	27.8	25.2	-162.2
	75	75	73.55	27.5
	100	100	79.32	29.1
1.0 M H_2SO_4	125	37.5	34.9	-140.8
	150	38.1	35.5	-141.8
	Blank	34.0	31.4	-132.7
	25	37.4	34.8	-125.3
	50	41.7	39.0	-114.9
	75	44.8	42.2	-107.5
	100	45.1	42.4	-108.7
	125	48.8	46.2	-99.1
	150	51.5	48.9	-93.3

3.5. Adsorption isotherm

The adsorption of organic inhibitor molecules from the aqueous solution can be considered as a quasi-substitution process between the organic compounds in the aqueous phase [$Org_{(sol)}$] and water molecules associated with the metallic surface [$H_2O_{(ads)}$] as represented by the following equilibrium [39]:

$$Org_{(sol)} + xH_2O_{(ads)} \longrightarrow Org_{(ads)} + xH_2O_{(sol)} \quad (11)$$

where x is the number of water molecules replaced by one organic molecule. In this situation, the adsorption of constituent compound of *G. tournefortii* extract was accompanied by desorption of water molecules from the mild steel surface. The corrosion adsorption processes can be understood using adsorption isotherm. The most frequently used adsorption isotherms are Langmuir, Temkin, and

Frumkin. So these adsorption isotherms were tested for the description of adsorption behavior of *G. tournefortii* extract on steel surface in HCl and H_2SO_4 solutions. The correlation coefficient, R^2, was used to choose the isotherm that best fit experimental data. The simplest, being the Langmuir isotherm, is based on assumption that all adsorption sites are equivalent and that particle binding occurs independently from nearby sites being occupied or not [45]. A correlation between surface coverage (θ) and the concentration (C) of inhibitor in the electrolyte can be represented by the Langmuir adsorption isotherm.

$$\frac{C}{\theta} = \frac{1}{K} + C \qquad (9)$$

where, K is adsorption equilibrium constant. The θ values calculated using weight loss data at 25-65 ºC for mild steel in 2.0 M HCl and 1.0 M H_2SO_4 with various concentration of *G. tournefortii* extract.

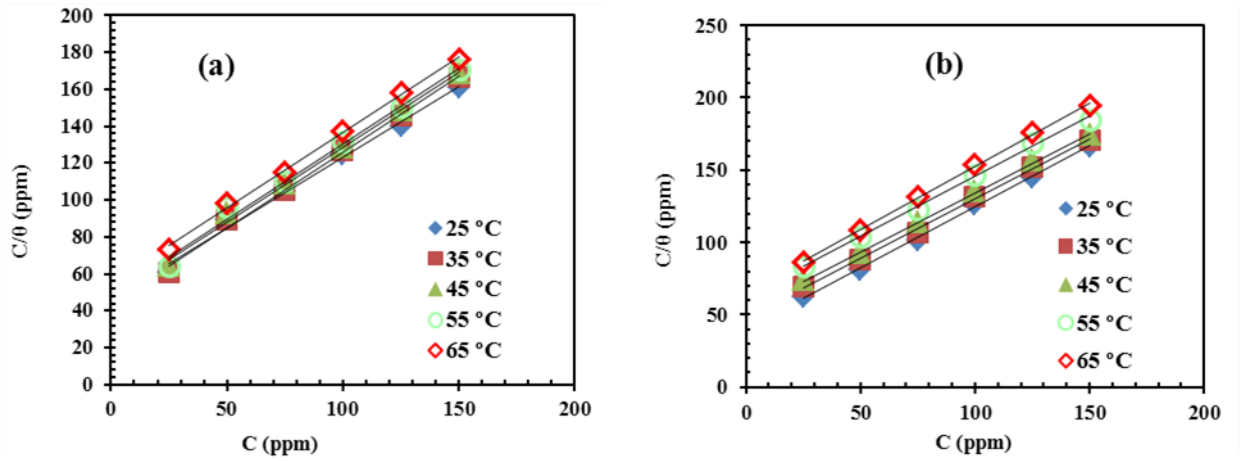

Figure 7. Langmuir isotherm for adsorption of *G. tournefortii* extract in (a) 2.0 M HCl and (b) 1.0 M H_2SO_4 solution on the mild steel surface.

The plots of C/θ vs. C yield straight lines with slopes close to 1 and the linear correlation coefficients are also close to 1 (Fig. 7), indicating that the adsorption of *G. tournefortii* extract on the mild steel surface in both acid solutions and for all temperatures is well fitted to the Langmuir adsorption isotherm. Langmuir adsorption isotherm assumes that the adsorbed species occupy only one surface site and there are no interactions with other adsorbed species [40]. Due to the unknown molecular mass of *G. tournefortii* extract, the energy of adsorption and thermodynamic parameters could not have been calculated.

3.6. Adsorption mechanism

To clarify the mechanism of inhibitor adsorption, it is necessary to establish the adsorption modes of the inhibiting species (whether molecular or ionic). The predominant adsorption mode will be dependent on factors such as the extract composition, type of acid anion as well as chemical

changes to the extract. The complex nature of the corrosion inhibition process is not in doubt. This complexity is increased by several orders of magnitude when one considers plant extracts with their complicated chemical compositions. This makes it difficult to assign the inhibitive effect to adsorption of any particular constituent [15, 41 and 42]. The caffeic acid derivatives including neochlorogenic acid (3-O-caffeoylquinic acid), cryptochlorogenic acid (4-O-caffeoylquinic acid), chlorogenic acid (5-O-caffeoylquinic acid), pseudochlorogenic acid (1-O-caffeoylquinic acid) and caffeic acid (CA) have been characterized [23] in *G. tournefortii* extract and the chemical structures is shown in Fig. 8. Inspection of Fig. 8 shows that these compounds contain many O atoms in functional groups and O–herterocyclic rings, which meets the general characteristics of typical corrosion inhibitors.

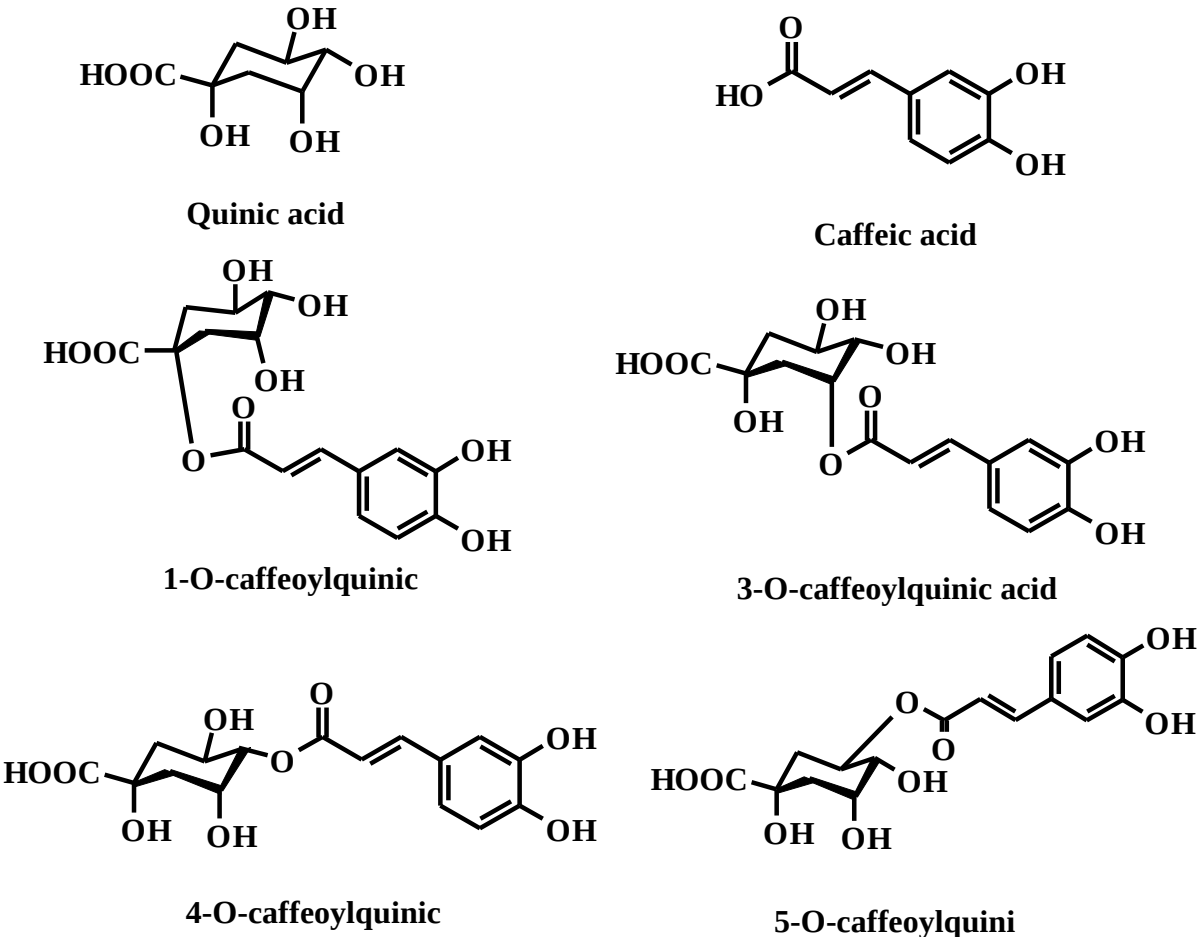

Figure 8. Some chemical structures of *G. tournefortii* extract components.

Thus, it is reasonable to deduce that the caffeic acid derivatives in *G. tournefortii* extract exhibit the inhibition performance. In the present study, our results are lack of isolating these compounds, thus it is not possible to determine what components present in *G. tournefortii* extract created their relatively high ability to inhibit corrosion. But we consider the absorption process from other directions. The data obtained from the temperature dependence of the inhibition process suggest a physical or coulombic type of adsorption. The physical adsorption mechanism results from electrostatic attractive forces between inhibiting organic ions or dipoles and the electrically charged

surface of the metal due to the electric field existing at the metal/solution interface. A negative surface charge will favour the adsorption of cations whereas anion adsorption is favoured by a positive surface charge. These main chemical compounds as shown in Fig. 8 might be protonated in acid media. A corroding mild steel specimen carries a positive surface charge in both sulphuric and hydrochloric acid solutions [43] and as such, protonated species should be poorly adsorbed. On the other hand, the ability of Cl^- ions in hydrochloric acid to be strongly adsorbed on the metal surface and hence facilitate physical adsorption of inhibitor cations is an important consideration. Accordingly, a comparison of the inhibiting characteristics of the extract in 2.0 M HCl and 1.0 M H_2SO_4 could very well give an insight into the mode of adsorption of the inhibiting species.

The acid anions of Cl^- and SO_4^{2-} could be firstly adsorbed; they create excess negative charge toward the solution, and favor more adsorption of the cations [44]. Then the protonated inhibitor may adsorb on the negatively charged metal surface through electrostatic interactions. In other words, there could be a synergism between anions (Cl^-, $SO4^{2-}$) and protonated inhibitor. The inhibitive ability of *G. tournefortii* extract in HCl is greater than that in H_2SO_4, which implies that the adsorption of inhibitor could be influenced by the nature of anions in acidic solutions. It is well known that Cl^- ions have stronger tendency to adsorb than do $SO4^{2-}$ions [45], and the electrostatic influence on the inhibitor adsorption may be the reason for an increased protective effect in halide-containing solution [46]. Moreover, the lesser interference of $SO4^{2-}$ions with the adsorbed protonated cations may lead to lower adsorption [45]. So, the adsorption of *G. tournefortii* extract on steel surface in HCl solution is stronger than that in H_2SO_4 solution, which leads to higher inhibition performance in HCl than that in H_2SO_4. When protonated chemical molecules in *G. tournefortii* extract are adsorbed on steel surface, a coordinate bond may be formed by partial transference of electrons from O atoms to vacant d orbits of Fe. Owing to lone-pair electrons of O atoms in *G. tournefortii* extract, *G. tournefortii* extract may combine with freshly generated Fe^{2+} ions on steel surface to form the metal inhibitor complexes. These complexes might get adsorbed onto steel surface by van der Waals force to form a protective film which keeps mild steel from corrosion.

4. CONCLUSION

G. tournefortii extract acts as a good inhibitor of corrosion of mild steel in both 2.0 M HCl and 1.0 M H_2SO_4 solutions. Inhibition efficiency value increases with the inhibitor concentration. Potentiodynamic polarization results revealed that *G. tournefortii* extract follows mixed type corrosion inhibition mechanism in both acid solutions. EIS exhibit one single capacitive loop in 2.0 M HCl; while a large capacitive loop at high frequencies (HF) followed by a small inductive loop at low frequencies (LF) in 1.0 M H_2SO_4. The addition of *G. tournefortii* extract in both acid solutions enhances R_{ct} values while reduces C_{dl} values. Temperature studies revealed a decrease in efficiency with rise in temperature and corrosion activation energies were higher in the presence of the extract. Comparative analyses of the results from both acid solutions suggest that protonated and neutral organic species in the extract may be responsible for the observed inhibitive behaviour, the predominant effect being the physical adsorption of protonated species.

ACKNOWLEDGEMENT
The financial support of research council of Payame Noor University of Isfahan is gratefully acknowledged.

References

1. Sh. Deng, Xianghong Li, Hui Fu, *Corros. Sci.* 53 (2011) 760.
2. A.S. Fouda, A.S. Ellithy, *Corros. Sci.* 51 (2009) 868.
3. M.J. Bahrami, S.M.A. Hosseini, P. Pilvar, *Corros. Sci.* 52 (2010) 2793.
4. Sh. Deng, X. Li, H. Fu, *Corros. Sci.* 53 (2011) 822.
5. RamazanSolmaza, EceAltunbas, GulfezaKardas, *Mater. Chem. Phys.* 125 (2011) 796–801.
6. Sh. Deng, X. Li, *Corros. Sci.* 55 (2012) 407.
7. O. K. Abiola, J.O.E. Otaigbe, O.J. Kio, *Corros. Sci.* 51 (2009) 1879–1881.
8. E.E. Oguzie, *Corros. Sci.* 49 (2007) 1527.
9. A.K. Satapathy, G. Gunasekaran, S.C. Sahoo, Kumar Amit, P.V. Rodrigues, *Corros. Sci.* 51 (2009) 2848.
10. M.A. Quraishib, AmbrishSingha, Vinod Kumar Singha, Dileep Kumar Yadavb, Ashish Kumar Singhb, Materials Chemistry and Physics 122 (2010) 114.
11. A.Y. El-Etre, Materials Chemistry and Physics 108 (2008) 278.
12. L.R. Chauhan, G. Gunasekaran, *Corros. Sci.* 49 (2007) 1143.
13. A.M. Abdel-Gaber, B.A. Abd-El-Nabey, M. Saadawy, *Corros. Sci.* 51 (2009) 1038.
14. M. Behpour, S.M. Ghoreishi, M. Khayatkashani, N. Soltani, Materials Chemistry and Physics 131 (2012) 621.
15. E.E. Oguzie, C.K. Enenebeaku, C.O. Akalezi, S.C. Okoro, A.A. Ayuk, E.N. Ejike, Journal of Colloid and Interface Science 349 (2010) 283.
16. A.M. Abdel-Gaber, E. Khamis, H. Abo-ElDahab, Sh. Adeel, Materials Chemistry and Physics 109 (2008) 297.
17. M. Lebrini, F. Robert, A. Lecante, C. Roos, *Corros. Sci.* 53 (2011) 687–695.
18. P.C. Okafor, M.E. Ikpi, I.E. Uwaha, E.E. Ebenso, U.J. Ekpe, S.A. Umoren, *Corros. Sci.* 50 (2008) 2310.
19. K.P.Vinod Kumar1, M. SankaraNarayanaPillai, G. RexinThusnavis, *J. Mater. Sci. Technol.* 27 (2011) 1143.
20. H. Z. Alkhathlan, M. Khan, M. M. Saeed Abdullah, A.M. Al-Mayouf, A. A. Mousa, Z. A. M. Al-Othman, *Int. J. Electrochem. Sci.* 9 (2014) 870.
21. S. Garai, S. Garai, P. Jaisankar, J.K. Singh, A. Elango, *Corros. Sci.* 60 (2012) 193.
22. Emeka E. Oguzie, *Corros. Sci.* 50 (2008) 2993.
23. Gh. Haghi, A. Hatami, R. Arshi, *Food Chemistry* 124 (2011) 1029.
24. I.B. Obot, N.O. Obi-Egbedi, S.A. Umoren, *Corros. Sci.* 51 (2009) 1868.
25. S.A. Ali, A.M. El Shareef, R.F. Al-Ghandi, M.T. Saeed, *Corros. Sci.* 47 (2005) 2659.
26. M.A. Kiani, M.F. Mousavi, S. Ghasemi, M. Shamsipur, S.H. Kazemi, *Corros. Sci.* 50 (2008) 1035.
27. H. Amar, A. Tounsi, A. Makayssi, A. Derja, J. Benzakour, A. Outzourhit, *Corros. Sci.* 49 (2007) 2936.
28. M. Lagrenee, B. Mernari, M. Bouanis, M. Traisnel, F. Bentiss, *Corros. Sci.* 44 (2002) 573.
29. A.K. Singh, M.A. Quraishi, *Corros. Sci.* 52 (2010) 152.
30. N. Labjar, M. Lebrini, F. Bentiss, N.E. Chihib, S. El Hajjaji, C. Jama, *Mater. Chem. Phys.* 119 (2010) 330.
31. X. Liu, Shenhao Chen, H. Ma, G. Liu, L. Shen, *Appl. Surf. Sci.* 253 (2006) 814.
32. M. Lebrini, F. Robert,C. Roos, *Int. J. Electrochem. Sci.,* 6 (2011) 847.

33. M. Behpour, S.M. Ghoreishi, N. Mohammadi, N. Soltani, M. Salavati-Niasari, *Corros. Sci.* 52 (2010) 4046.
34. A.M. Fekry, R.R. Mohamed, *Electrochim. Acta* 55 (2010) 1933.
35. K. Tebbji, N. Faska, A. Tounsi, H. Oudda, M. Benkaddour, B. Hammouti, *Mater. Chem. Phys.* 106 (2007) 260.
36. S. Zor, B. Yazici, M. Erbil, *Corros. Sci.* 47 (2005) 2700–2710.
37. M.S. Morad, *Corros. Sci.* 50 (2008) 436–448.
38. R. Solmaz, G. Kardaş, M. Çulha, B. Yazıcı, M. Erbil, *Electrochim. Acta* 53 (2008) 5941.
39. N.A. Negm, N.G. Kandile, E.A. Badr, M.A. Mohammed, *Corros. Sci.* 65 (2012) 94–
40. 103.
41. M.A. Hegazy, A.S. El-Tabei, A.H. Bedair, M.A. Sadeq, *Corros. Sci.* 54 (2012) 219.
42. F. Zucchi, I.H. Omar, *Surf. Technol.* 24 (1985) 391.
43. E. E. Oguzie, *Mater. Chem. Phys*. 99 (2006) 441.
44. F. Bentiss, M. Traisnel, M. Lagrenee, *Corros. Sci.* 42 (2000) 127.
45. X. Li, Sh. Deng, H. Fu, *Corros. Sci.* 62 (2012) 163.
46. F. Bentiss, M. Traisnel, N. Chaibi, B. Mernari, H. Vezin, M. Lagrenee, *Corros. Sci.* 44 (2002) 2271.